Article:

Craig, TJ orcid.org/0000-0003-2198-9172 and Copley, A (2018) Forearc collapse, plate flexure, and seismicity within the downgoing plate along the Sunda Arc west of Sumatra. Earth and Planetary Sciences Letters, 484. pp. 81-91. ISSN 0012-821X

https://doi.org/10.1016/j.epsl.2017.12.004

Forearc collapse, plate flexure, and seismicity within the downgoing plate along the Sunda Arc west of Sumatra – Accepted manuscript, authors version

T. J. Craig[1,*], A. Copley[2]

[1] Institute of Geophysics and Tectonics,
School of Earth and Environment, University of Leeds,
Leeds, LS2 9JT, UK
[2] Bullard Laboratories,
Department of Earth Sciences, University of Cambridge,
Madingley Road, Cambridge, CB3 0EZ, UK.
*Corresponding author: t.j.craig@leeds.ac.uk

December 3, 2017

Abstract

Deformation within the downgoing oceanic lithosphere seawards of subduction zones is typically characterised by regimes of shallow extension and deeper compression, due to the bending of the oceanic plate as it dips into the subduction zone. However, offshore Sumatra there are shallow compressional earthquakes within the downgoing oceanic plate outboard of the region of high slip in the 2004 Aceh-Andaman earthquake, occurring at the same depth as extensional faulting further seaward from the trench. A clear separation is seen in the location of intraplate earthquakes, with extensional earthquakes occurring further seawards than compressional earthquakes at the same depth within the plate. The adjacent section of the forearc prism west of Aceh is also anomalous in its morphology, characterised by a wide prism with a steep bathymetric front and broad, gradually-sloping top. This shape is in contrast to the narrower and more smoothly-sloping prism to the south, and along other subduction zones. The anomalous near-trench intraplate earthquakes and prism morphology are likely to be the result of the geologically-rapid gravitational collapse of the forearc, which leads to induced bending within the subducting plate, and the distinctive plateau-like morphology of the forearc. Such collapse of the forearc could be caused by changes through time of the material properties of the forearc rocks, or of the thickness of the sediments entering the subduction zone.

Highlights:

- Near-trench intraplate compressional seismicity is observed in the downgoing plate
- Earthquakes are indicative of near-trench unbending of the lithosphere
- Seismicity and forearc morphology are consistent with gravitational forearc collapse

Keywords: Sumatra, intraplate seismicity, forearc deformation, flexure

1 Introduction

On 24th December 2004, the M_W 9.2 Aceh-Andaman earthquake ruptured a section of the subduction interface along the Sunda arc stretching from Simeulue island, west of Sumatra, northwards to the Andaman islands, ~1300 km along strike (Figure 1; Ammon et al., 2005; Rhie et al., 2007; Chlieh et al., 2007). Most major subduction-interface earthquakes are followed by the widespread rupture of normal faults in the downgoing plate seawards of the trench (e.g., Lay et al., 1989, 2009; Craig et al., 2014a). These earthquakes are the result of the release of shallow extensional stresses in the outer rise region of the downgoing plate as it bends into the subduction zone. However, the 2004 Aceh-Andaman earthquake is so far unique in the observational record in that it was followed by shallow compressional, rather than extensional, seismicity beneath the trench and under the outer trench slope/outer rise, along with only a small number of normal-faulting aftershocks within the downgoing plate (Dewey et al., 2007).

The near-trench compressional seismicity offshore Sumatra has variously been interpreted as the transfer of the active subduction interface from the top of the downgoing plate into the mantle of the downgoing plate (Singh et al., 2008), as a shallow response within the downgoing plate to high levels of induced stress at the updip termination of the 2004 mainshock rupture on the interface, or as shallow motion on splay faults branching up from the main interface (Dewey et al., 2007). However, correctly understanding the tectonic significance of these earthquakes relies on accurately estimating their locations, depths, and mechanisms. The determination of accurate estimates for the location of these intraplate earthquakes, at a resolution beyond routine global seismological techniques, is therefore of vital importance. Similarly, one of the most accurate ways of constraining the location of the active subduction megathrust – critical for determining which earthquakes are truely intraplate – is through the precise location of low-angle thrust-faulting earthquakes that lie on this interface. In the first part of this study, we therefore present the results of body-waveform modelling to constrain the source parameters of the near-trench seismicity offshore Sumatra (Figure 1), in order to image the deformation field within the downgoing oceanic plate.

In the second part of this study, we investigate the links between our seismological results and the structure and morphology of the forearc prism. The Sunda Arc is notable for both its variable forearc morphology along strike (McNeill and Henstock, 2014), and major along-strike variations in the thickness of sediments on the downgoing plate (Figure 1e, see also compiled data in Table 1 of McNeill and Henstock 2014). Incoming sediment thickness varies from 1 – 5 km, with the greatest thickness occurring along a section of the trench stretching north from Simeulue island (2.6°N, 96.0°E) to approximately 6.5°N, and overlaps with the region of highest slip in the 2004 earthquake. In this area, west of northern Sumatra, the forearc is characterised by a wide forearc prism with a relatively low-gradient top and steep frontal slope (Figure 2e – h), in contrast to the region to the south (Figure 2i,j) where the prism is characterised by the more gently-sloping rise from the trench over a wider across-strike extent.

The morphology and internal structure of a forearc prism is controlled by a number of competing factors, including the dip and physical properties of the subduction interface, the material properties of the over-riding accretionary wedge, the thickness and character of incoming sediments, and the degree to which they are accreted onto the frontal prism, underplated onto the base of the prism, or subducted along with the downgoing plate. Whilst the growth and evolution of accretionary prisms is often treated as being uniform through time, we investigate how changing some of the properties governing its shape (specifically, incoming sediment thickness or internal rheology) can lead to a relatively rapid readjustment in the prism shape, which also leads to a concurrent adjustment of the induced stress field within the downgoing plate. We then present a conceptual model linking the morphological evolution of the forearc prism to the changing stress distribution within the downgoing plate, as mechanism to explain both the anomalous prism morphology and the unique distribution of seismicity.

2 Seismicity

2.1 Modelling

We here determined earthquake source parameters for events along the Sunda arc, in close proximity to the trench, by the inversion of long-period body waves using the algorithm of Zwick et al. (1994). The workflow followed is similar to that described in detail in Tilmann et al. (2010) and Craig et al. (2014a). Teleseismic *P*- and *SH*-waves were inverted over a time window encompassing the direct arrival (*P, S*) and subsequent principal depth phases (*pP, sP, sS*) to determine the source mechanisms, centroid depth and seismic moment of earthquakes with $M_W \geq 5.5$ since 1990. Examples are shown in Supplementary Figures 1 and 2.

For events occurring seawards of the trench, a source-side velocity structure was used consisting of a crustal layer 7 km thick ($V_P = 6.5$ ms^{-1}, $V_S = 3.8$ ms^{-1}, and $\rho = 2800$ kg m^{-3}) over a mantle halfspace ($V_P = 8.1$ m s^{-1}, $V_S = 4.6$ m s^{-1}, and $\rho = 3300$ kg m^{-3}). To compensate for the laterally varying thickness and seismic velocity structure of the accretionary wedge landward of the trench, the crustal layer thickness is increased and the velocities and density reduced with increasing distance from the trench, in-line with the results of refraction profiles across the region (Dessa et al., 2009; Singh et al., 2012). In each case, this velocity structure is overlain by a water layer with the water depth in the source region being initially based on the SRTM30PLUS bathymetric models (filtered to remove wavelengths of less than 10 km), and adjusted if required to best fit any observed water multiples, although the inversion window is limited where possible to exclude further water multiples after the sP arrival. The inclusion of horizontally-polarised S-waves aids in minimising the effects of any inaccuracies (or azimuthal variability) in water depth on the depth determination of the earthquake, as the horizontal polarisation excludes and converted P-wave phases from featuring in the waveform coda. The restricted frequency content of the long period P-wave data also reduces the P wave sensitivity to water depth (Engdahl and Billington, 1986).

Direct P- and S-wave arrivals were manually picked from broadband seismograms in each case. The earthquakes modelled are shown in Figure 1 and listed in Table S1, and include the majority of events with $M_W \geq 5.5$ occurring in the study area within 400 km of the trench. The exceptions are in the period immediately following the mainshock ruptures of the Aceh-Andaman and Nias earthquakes, in late December 2004 and late March 2005 respectively, as the signals from smaller-magnitude aftershocks during the initial hours after the mainshocks were swamped by the mainshock coda, and failed to yield robust results.

Typical uncertainties in source mechanism are on the order of 10° for strike and rake, and 5° for dip (e.g. Molnar and Lyon-Caen, 1989; Taymaz et al., 1991; Craig et al., 2014b). Depth uncertainties, of most direct relevance to this study, are usually $\sim \pm 3$ km (Tilmann et al., 2010), much of which derives from the velocity model used. Hence, relative uncertainties between earthquakes in the same geographic location are often smaller. Accounting for increased uncertainty in the depth estimates due to bathymetric variation around the source, and the differing effect this has on the depth phases for stations with different bouncepoints, we estimate a further increase in uncertainty for events near sharp bathymetric variations of $\sim$1 km for the deepest of our studied events, although we note that due to the increasing moveout of the depth-phase bouncepoints with increasing source depth, this uncertainty is itself depth-dependent.

Whilst the focus of this work is on deformation in the downgoing plate, it is also necessary to determine source parameters for low-angle thrust-faulting aftershocks associated with motion on the main subduction interface, so as to correctly define the location of this interface, and to determine whether events were in the downgoing plate or within the overlying accretionary wedge. Hence, a large number of the low-angle thrust-faulting earthquakes shown on Figures 1a & 1d are in fact on the plate interface, and not within the downgoing plate. To supplement these events in determining the location of the plate interface, we also draw upon a detailed study of large-magnitude interface aftershocks at the southern end of the study area that was conducted by Tilmann et al. (2010), along with three microseismic surveys conducted in the aftermath of the major interface events of 2004 and 2005 (black points on Figures 2a and 3; Lin et al. 2009; Lange et al. 2010; Tilmann et al. 2010). In using the results from local seismic networks, we only show earthquakes located within the area covered by the network, and well constrained events that are based on observations at multiple ($\geq$ 5) stations of both P and S arrivals.

2.2 Earthquake distribution

Seismic activity in the study area is shown on Figure 1, and is dominated by thrust-faulting earthquakes, many of which show a low-angle, northeast-dipping nodal plane consistent with motion on the main subduction interface around the margins of the mainshock slip patch (Figure 1e). Mechanisms in the area around the boundary between the 2004 and 2005 source regions, previously determined by Tilmann et al. (2010), are all also consistent with low-angle thrust-faulting seismicity on the subduction interface (indicated by the larger green points on Figure 1a).

A large number of low-angle thrust-faulting earthquakes also occur beneath the Aceh basin region (Figure 1d). Previous studies have suggested that these may represent motion on a splay fault (Waldhauser et al., 2012) or the reloading and repeat rupturing of small asperities within a section of the interface otherwise undergoing aseismic afterslip (Yu et al., 2013). However, whilst we do find a slight deepening of these earthquakes with distance from the trench, we find insufficient difference between the depths and mechanisms of these earthquakes to distinguish between these possible causes.

There are also a number of thrust-faulting mechanisms beneath and seawards of the trench with orientations (in particular, dip angles) that are inconsistent with motion on a low-angle subduction interface (Figure 1a). Whilst these earthquakes are found in a range of locations along the trench, a major concentration occurs at $\sim 2.5°$N, with a range of focal mechanism orientations, and depths of 6 – 26 km below the seafloor (Figure 1a). This cluster lies to the south of the region of highest slip in the 2004 mainshock (Figure 1e), and in the region of thickest sediment on the incoming plate (Figure 1e), and is the main subject of the next section.

In contrast to the widespread thrust-faulting earthquakes, normal-faulting mechanisms are sparse (Figure 1b), with only 10 near-trench normal-faulting events with $M_W > 5.5$, nine of which have occurred since the 2004 mainshock are present in our catalogue, and all of which are indicative of bending-driven horizontal extension within the shallow outer-rise or outer-trench slope region as observed in other subduction zones (Christensen and Ruff, 1988; Craig et al., 2014a). Three normal-faulting earthquakes have also occurred significantly landward of the trench, one indicating deeper extension within the downgoing plate, and two indicating extension at the base of the forearc, at depths within error of the inferred plate interface.

In the last decade, there have been a number of major strike-slip earthquakes located in the interior of the Indian plate, including the M_W 8.7 April 2012 earthquake (e.g. Yue et al., 2012), associated with a region of diffuse deformation in the Wharton basin (Delescluse et al., 2012; Aderhold and Abercrombie, 2016). Strike-slip seismicity in our study region, both seawards and landwards of the trench, follows a general trend of NNE-SSW and

ESE-WNW aligned nodal planes (Figure 1.c). The alignment of the approximately north-south nodal planes with oceanic fracture zones in this region (Figure 1.c,f), and the identification of lineations in microseismic activity beneath the accretionary wedge (Lange et al., 2010), indicate the widespread reactivation of the pre-existing oceanic fabric, both seaward and landward of the trench, consistent with a detailed study of Indian Ocean seismicity in this region (Aderhold and Abercrombie, 2016). Two of the events on Figure 1.c, at ∼5.75° N 93.25° E, lie along-strike from the 2012 Indian Ocean earthquakes, and may represent continued deformation of the same fracture zone beneath the accretionary wedge. Shallower strike-slip seismicity landwards of the trench is concentrated along the Sumatran and West Andaman fault systems, which accommodate the strike-slip componeent of the oblique convergence between the Indian Ocean and Sunda.

Little conclusive evidence is seen within the region for large-scale seismic activity within the forearc prism, outside of these major strike-slip systems (Figure 1 and Figure 3). Previous studies have suggested that the accretionary wedge in this region may undergo either gravity-driven extension and collapse (M^{c}Kenzie and Jackson, 2012), or compressional motion on splay faults following the mainshock (Chauhan et al., 2009). Both of these mechanisms might be expected to be expressed in the seismicity within the accretionary prism. Of the normal-faulting earthquakes analysed here, none locate conclusively within the accretionary prism, although the depths of only a small number of the normal-faulting earthquakes recorded in the gCMT catalogue (blue triangles, Figure 1b) for the forearc region could be confirmed using the waveform modelling techniques employed here. This difficulty arises because many of these events occurred in the time period directly following the mainshock, when continuing seismic coda from the mainshock prevents a robust inversion using bodywaves. A single high-angle thrust at 3.9° N, 95.3° E is confirmed to occur at a depth placing it in the accretionary prism (see Figure 1a), and this might represent seismogenesis on recently active splay faults within the prism (Graindorge et al., 2008; Chauhan et al., 2009), but it is unclear how widespread such deformation is. Presently-available seismological observations are therefore not able to unambiguously constrain the orientation of the principal strains within the accretionary wedge. However, the small number of earthquakes imply that much of the strain is likely to be accommodated aseismically.

2.3 Seismicity within the downgoing plate

As described above, much of the seismicity offshore Sumatra represents motion on the subduction interface. However, the near-trench intraplate seismicity, particularly the cluster of thrust-faulting earthquakes at $\sim 2.5°$N, present an important contrast to globally observed patterns of seismicity within the downgoing plate of subduction zones (Chapple and Forsyth, 1979; Christensen and Ruff, 1988; Craig et al., 2014a). On a global scale, normal faulting seaward of the trench is typically observed from the surface of the downgoing plate down to some transition depth, below which the plate either becomes aseismic, or switches to thrust-faulting earthquakes. This pattern, with shallow extension overlying deeper compression, is consistent with the accummulation of horizontal extensional strain along the top of the strong lithospheric plate, and horizontal compression along the base, as the plate itself bends into the subduction zone. Such bending-related strain, although accommodated by seismogenic brittle failure on faults, is expected to be recovered further on in the subduction process, as the subducting slab returns to being roughly planar as it descends into the upper mantle. This unbending of the slab downdip of the interface seismogenic zone is a common interpretation of the focal mechanisms of double seismic zones downdip of the seismogenic subduction interface (Engdahl and Scholz, 1977; Kao and Chen, 1996; Gamage et al., 2009). The location of the transition between bending and unbending is difficult to constrain, but in most subduction zones where it can be observed, it occurs significantly landward of the trench, and shallow normal-faulting earthquakes indicative of horizontal extension due to bending persist from the outer rise region to the trench (Craig et al., 2014a).

On Figures 2a and 3, we separate the seismicity of the subducting system into three geographic sections (divided by the green dotted lines on Figure 2a), and plot earthquake depth profiles as a function of distance to the trench for each section (Figure 3). We analyse the seismicity of each of these profiles from south to north in turn, and assess how they compare with the global pattern of seismicity within the downgoing plates at subduction zones:

1. South of 1.5°N (Figure 3c) the plate interface (approximated by the grey lines on Figure 3) is clearly delineated by a line of low-angle thrust-faulting earthquakes (see Figure 1a and Tilmann et al. 2010). The two normal-faulting events in this area are both trench-parallel. The shallowest one is consistent with bending-related extension seaward of the trench. The deeper event, located just landward of the trench, may indicate either that extension extends to 30 km into the plate, or may indicate a transition to unbending (with extension at the base of the plate), as the plate straightens out under the forearc. It is interesting to note that the location of both extensional earthquakes (in depth and across-strike distance) is matched by a cluster of microearthquakes imaged by Lange et al. (2010).

2. Between 1.5°N and 6.5°N (Figure 3b), a more complex pattern of seismicity is seen. The subduction interface is clearly delineated at > 50 km from the trench by a combination of low-angle thrust-faults (both those beneath the Aceh basin, and others further south) and microseismic aftershocks beneath Simeulue (green circles; Tilmann et al., 2010). At ~ 50 km seaward from the trench, a single shallow normal-faulting earthquake at 6 km depth is consistent with the typical model for shallow extension due to outer-rise bending (Chapple and Forsyth, 1979; Christensen and Ruff, 1988). Beneath this, a thrust-faulting earthquake at 40 km is consistent with compression in the deeper part of the bending plate, but the orientation of this mechanism is near-perpendicular to the trench, possibly instead reflecting along-strike curvature of the plate as the trench changes strike west of Northern Sumatra. In close proximity to the trench itself, seismicity is characterised by widespread thrust-faulting, extending from the surface down to > 30 km. This observations is, to our knowledge, unique in the world's subduction zones during the instrumental period (Craig et al.,

2014a). The widespread depth extent of these earthquakes is inconsistent with the idea that they might be concentrated onto a single low-angle structure (the subduction interface), and some of them must represent brittle failure in horizontal compression within the upper sections of the downgoing plate. The juxtaposition of these thrust and normal earthquakes shows a horizontal transition from shallow extension (the normal fault) to shallow compression (the thrust faults) as the trench is approached, as discussed below.

3. North of 6.5°N (Figure 3a), more sparse thrust-faulting earthquakes again serve to illuminate the subduction interface. In the near-trench region, two clusters of normal-faulting earthquakes at shallow depth ($<$ 25 km) within the oceanic plate occur with mechanisms sub-parallel to the trench, indicating bending-related faulting. Thrust-faulting earthquakes within 20 km of the trench occur at depths of 10 – 20 km, and with steeper dips than the interface events further landward. The depth extent over which we find these thrust-faulting earthquakes, and the variability in the orientation of their mechanisms (see Figure 1a) is inconsistent with all of them being focused on the main plate interface. However, the true interpretation of these events is uncertain – their depths suggest deformation similar to that seen over a larger depth interval on Figure 3b, and suggest that at least some of these earthquakes lie in the upper part of the downgoing plate. However, the more limited depth extent, and the lack of thrust-faulting earthquakes deeper than 16 km, means that we cannot rule out the possibility that these earthquakes represent either near-trench splay faulting, or compression in the frontal section of the forearc accretionary prism.

In summary, the southern section of our study area shows seismicity consistent with the globally-observed pattern for outer-rise regions, of bending-related shallow extension. The area west of Aceh, however, does not, and is instead characterised by the occurrence of thrust-faulting earthquakes within 20 km of the trench (both landwards and seawards) at a range of depths from 6 km to over 30 km (Figure 3b). This observation is inconsistent with interpretations that these earthquakes all occurred on the subduction interface, that they occurred on shallow splay faults branching upwards from the interface, or that they represent internal deformation within the toe of the forearc prism. The northernmost section of our study area may fit with the trend seen west of Aceh, but more limited seismicity, along with moderate-depth extension in the downgoing plate, mean we cannot rule out other deformation scenarios.

The shallow compressional seismicity within the downgoing plate occurs in an area where bathymetric surveys show evidence for well-developed trench-parallel normal faults breaking the top surface of the downgoing plate (Cook et al., 2014). The near-juxtaposition of these contrasting deformation indicators suggests a change in deformation through time, from the extension that produced the bathymetric scarps, to the presently-active faults that can be seen in the earthquake activity. Whilst the stress state within the downgoing plate is expected to vary, up to a point, across the interface seismic cycle, no evidence has been found elsewhere in the world for an outer rise region failing in both extension and compression either side of a major earthquake on the adjacent interface, despite an exhaustive search of recent outer-rise seismicity (Craig et al., 2014a). Additionally, the vast majority of the seismicity included in our study occurs in the years following the 2004 and 2005 interface events (see Supplementary Figure 2), at a time in the interface seismic cycle when the stress state within the downgoing plate oceanwards of the interface rupture patch is expected to be at its most extensional. The temporal evolution of stress is therefore presumably a longer-term effect, beyond the timescales of individual megathrust earthquake cycles.

This apparently-flexural seismicity within the downgoing plate is distinct from the intraplate deformation seen within the Wharton Basin (Wiens et al., 1985; Delescluse and Chamot-Rooke, 2007; Carton et al., 2014). This is particularly clear when considering the difference between the orientation of P- and T-axes for the near-trench thrust faulting, and the strike-slip faulting that dominates the internal deformation of the Wharton Basin. P-axes for the strike-slip faulting are orientated roughly NNW-SSE – approximately parallel to the strike of the subduction zone. In contrast, P-axes for the near-trench thrust-faulting earthquakes are orientated ENE-WSW, roughly perpendicular to that seen in the strike-slip faulting. We hence consider the causative process behind the near-trench seismicity to be distinct from that leading to the diffuse intraplate deformation of the Wharton basin. 2D seismic reflection studies have indicated the presence of small-offset faults within the Indian Ocean plate SW of Aceh (Carton et al., 2014), likely penetrating down into the oceanic mantle. Given the limitations of 2D seismic surveying, the orientation and true dip of these faults remains uncertain. However, their location and probable moderate dip angle suggests that they are not compatible with the deeper thrust-faulting seismicity discussed here, which occurs at either steep or shallow dip angles (depending on which nodal plane is the true fault plane), and closer to the trench.

3 Forearc evolution and stresses in the downgoing plate

The highly unusual oceanic intraplate seismicity described above occurs in a location also noted for its unusual forearc morphology, discussed in detail elsewhere (Kopp et al., 2008; McNeill and Henstock, 2014; Moeremans et al., 2014; Cook et al., 2014). Figure 2 shows across-strike averaged bathymetric profiles through a range of trench-perpendicular swaths, shown on Figure 2a, consistent with the available prism transects of ship-board bathymetry and 2D seismic data (see Figure 4 of McNeill and Henstock 2014). In the region of shallow oceanic intraplate compression (1.5°N – 6.5°N), the forearc shows a distinctive and unusual shape with a relatively flat top and sharp, steeply-sloping wedge-front (see Figure 2) characterised by the presence of landward-vergent folds (Henstock et al., 2008; McNeill and Henstock, 2014; Cook et al., 2014). In comparison, to the south of this region, the forearc shows the more commonly-observed shape of a relatively smoothly-sloping prism front from the trench up onto the prism top (Figure 2b-d). Additionally, following the definitions of McNeill and Henstock (2014), wherein the prism is defined as extending from the trench to edge of the forearc basin (often bounded by a margin-parallel fault system) the total prism width in this region is significantly wider ($\sim$150 km) than is is to the north or south ($\sim$100 km). The relatively flat plateau top through this region typically comprises 100 – 140 km of this total width. This leads to a prism with a distinct, sharp change in gradient $\lesssim$50 km landwards from the trench. In contrast, the section to the south is charactered by a much narrower prism ($\lesssim$120 km), with a gently curved slope profile (Figure 2i,j).

The northern section (Figure 2b–d) shows an extemely wide prism with a low angle, gradually sloping prism front. Given the ambiguous nature of both the seismicity and prism morphology of this northern section, likely complicated by the increasing proximity to both the Andaman spreading centre and the Bengal fan, we do not discuss it further here, but instead focus on the difference between the central and southern sections, and the transition between them near 1.5°N.

Next, we describe a dynamic model which is designed to investigate the potential causes of the unusual intraplate seismicity and forearc morphology. Based on the prevalence of ductile deformation features within the forearc wedge (i.e. folds), and the absence of significant seismicity, we model the forearc wedge using a viscous rheology (which is what would result from fluid-assisted pressure-solution/diffusion creep in the thick sedimentary pile (e.g. Rutter, 1983)). We will initially describe some simple two-parameter models that capture the governing physics of the accretionary wedges, before discussing a more complex multi-parameter thermomechanically-coupled model of our suggested mechanism for the evolution of the Sumatra forearc.

In our models, the accretionary wedge is underlain by the subduction megathrust, which we model as a constant-shear-stress lower boundary to the deformation within the wedge. The model consists of convergence between the rigid oceanic plate, and a deformable sedimentary veneer, with a rigid 'backstop' that represents the rigid part of the over-riding plate, against which the internally-deforming forearc prism builds a forearc wedge from the accumulation of the incoming deformable sediment (the model geometry is shown in Figure 4a). We solved the equations for low-Reynolds number fluid flow using the finite-difference methods described in Reynolds et al. (2015).

We non-dimensionalise the equations for Stokes flow using the thickness of sediment on the downgoing plate as the length-scale (H on Figure 4a), and the incoming plate velocity (u_0 on Figure 4a). The deformation is then governed by the equations

$$\nabla' h' = \alpha \nabla'^2 \mathbf{u}' \tag{1}$$

$$\alpha = \frac{\eta u_0}{\rho g H^2} \tag{2}$$

where h is the surface elevation, $\mathbf{u}$ is the velocity vector, η is the prism viscosity, ρ its density, g the gravitational acceleration, and primes denote non-dimensional quantities. In our model, we then solve of Eq. 1 in cross section only. α is analogous to the inverse of the Argand number (commonly used to described the viscous deformation of continental collision zones; England and McKenzie 1982), and represents the ratio of the stresses required to deform the wedge and the gravitational forces acting upon it. The other quantity in our model setup is the shear stress on the base of the wedge (τ_m, non-dimensionalised as $\tau'_m = \tau_m H/\eta u_0$), which appears as the lower boundary condition on our model domain. Where the shear stress on the bottom boundary is below τ_m, the sediments remain mechanically attached to the downgoing plate (i.e. a horizontally-rigid lower boundary condition), and deform by internal shearing of the sedimentary package. Where the shear stress reaches τ_m, the boundary condition is imposed such that there is sliding on the fault at the base of the wedge, with the velocity required for the shear stress on the base of the overlying material to equal τ_m.

The growth of the forearc wedge is a balance between the stresses on the base (τ_m) that are able to support the overlying topography, and gravity acting to reduce the elevation of the wedge by lateral spreading. If τ and α remain constant through time, the balance between these effects leads to a wedge that grows in a close to self-similar manner. This situation is the viscous equivalent of a 'critical taper' coulomb wedge. Such a model is shown in Figure 4b for the case where the stresses on the subduction thrust dominate the growth of the prism, with little deformation occurring in response to topographic forces until when the prism height is roughly five times larger than the incoming sediment thickness (upper line on the figure).

In our modelling approach we can investigate the lateral and temporal variations in the style of strain that result from changes in the model parameters. Figure 4c shows the effect of reducing the value of α by a factor of 10, with the starting topography in the model given by the red line in Figure 4b. The wedge undergoes gravitational collapse, the front rapidly advances, and the topography develops a low-gradient top and a steeper front. The rate of propagation of the prism slows down as a new dynamic balance between the forces acting upon it is approached. It is therefore clear that changes in the value of α can result in rapid transient propagation of the wedge, and a change in the overall morphology.

A number of effects could change the value of α (Eq. 2). The most likely reason for a dramatic change in α is due to a change in the viscosity of the wedge. In shallow sedimentary sections, the viscosity for rocks deforming by solution-precipitation creep (i.e. diffusion creep) is highly dependent on temperature, and so on depth. This effect arises because the viscosity is governed by an Arrhenius relation, as with other creep mechanisms (i.e. $\eta = A\exp(-E/RT)$, where A is a constant, E is the activation energy, R is the gas constant, and T is temperature) (Rutter, 1983; Connolly and Podladchikov, 2000). In slowly-deposited deep-sea sediments, the thermal profile is in equilibrium, so depth is a proxy for temperature. The exponential term in the expression for viscosity can lead to dramatic changes in viscosity over small depth intervals. For example, Connolly and Podladchikov (2000) modelled a decrease in viscosity of over 1.5 orders of magnitude between depths of 1 and 2 km. The appearance of dramatically lower-viscosity sediments being input into the wedge, because of kilometre-scale increases in the incoming sedimentary thickness, would make dramatic changes to the average viscosity of the wedge on short timescales, and could lead to the effects modelled above because of the dramatic reduction in α.

Decreases in the rate of convergence with time could also reduce the value of α. This effect would reduce the rate of sediment input, and so lead to collapse of the wedge. However, it is unlikely that the convergence in Sumatra has changed significantly in recent times (DeMets et al., 2010), and such a change would affect the entire arc, rather than only one section of it.

There are unlikely to be major temporal changes in the density of the wedge because of the limited variation in the density in the incoming sediments, which is considerably less and an order of magnitude. The thickness of the incoming sediments appears in the expression for α, as a separate effect from the thermal and viscosity effects discussed above. A sudden change in α could be interpreted as a change in the incoming sediment thickness. However, because H enters into the expression for α as $1/H^2$, and the viscosity depends on $\exp(-E/RT)$, where $T \propto H$, we are likely to be in a regime where the exponential term is more dominant than the quadratic, and so the viscosity effects discussed above are more important in this setting.

Changing the value of τ_m (basal shear stress) can also lead to the outwards growth of the prism. However, this occurs as a shallowing of the roughly constant-gradient wedge front seen in 4b, failing to produce a steep front to the evolving prism (Figure S4), and therefore is less consistent with the morphology of the Sumatra forearc west of Aceh than decreasing the value of α.

The gravitational collapse of the wedge as shown in Figure 4 will affect the stress-state of the underlying oceanic plate (Figure 5). If the outwards propagation of the wedge is more rapid than the rate at which the subducted slab can 'roll back' through the mantle, the wedge collapse and the propagation of the collision front out over the incoming plate will result in the zone of bending moving ocean-wards, and the creation of a region of opposite-polarity un-bending close to the nose of the wedge. In this location, where the oceanic plate flattens under the propagating thrust belt, previously accrued extensional strain is recovered through shallow compression within the downgoing plate (Figure 5). Changing α therefore provides a mechanism to explain both the highly unusual oceanic intraplate seismicity and the distinctive forearc morphology offshore Sumatra. The precise nature of the induced stress field remains uncertain, due to the rheological complexity of the downgoing plate, and remaining uncertainties in the response of faults to applied stresses. However, given the magnitude of the change in the overriding topography, the stresses produced are likely to be on the order of 100's MPa – far greater than observed stress drops in intraplate earthquakes, and therefore easily sufficient to influence the pattern of bending-related deformation and seismicity that we observe.

The simple two-parameter model discussed above captures the dominant controls on the behaviour of accretionary wedges, without the added parameters that arise in a fully thermomechanically-coupled model. In order to demonstrate this point, in the supplemental information we include a model for the evolution of the temperature and deformation within the forearc in which thermomechanical coupling has been implemented (see Figure S5). The complexity of this model, in terms of the wide range of free parameters with unknown values, means that it does not provide any additional insights into the evolution of accretionary wedges. However, it is included to demonstrate that the results of our two-parameter model, which point towards collapse of the Sumatran forearc in response to an influx of thick, hot, and weak sediment, are mirrored by more complex models.

4 Controls on forearc equilibrium

The question remains as to which of the potential controlling factors (prism viscosity or incoming sediment thickness) may have changed significantly in the geologically recent past in the region of Aceh. Internal prism viscosity is expected to evolve over time as the prism builds up, changing its internal thermobarometric state. However, this evolution will proceed slowly, on the timescale of prism formation, and the prism geometry would be expected to evolve gradually to maintain an equilibrium with the evolving viscosity (see Figure S5). The presence of anomalous intraplate seismcity in the outer rise region, along with the development of the unusual forearc morphology, suggests a more rapid gravitationally-driven collapse.

The input of relatively warm and low-viscosity sediments into the wedge, due to a change in sediment thickness on the incoming plate, provides a mechanism for the prism to undergo rapid collapse. Incoming oceanic sediment thickness is largely a function of three parameters: plate age (and hence pelagic sediment thickness), proximity to clastic sediment sources, and geographic relation to basin-bounding features (e.g., fracture zones). In the case of the Sunda Arc, variation in clastic sediment input and composition are relatively small along strike, south of the region of influence of the Bengal fan, which reaches down to the approximate latitude of the Nicobar islands ($\sim 11°$N). Although the age of the incoming plate varies across our study area by approximately 30 Myrs, the dominant influence on sediment thickness is the structural segmentation of the downgoing plate by fracture zones, and the major features of the Ninety East ridge and the fossil spreading ridge that intersects the trench at $\sim 0.5°$N. Figure 1e summarises the known constraints on the sediment thickness at the trench (McNeill and Henstock, 2014, and references therein), and demonstrates that sediment thickness along this section of the arc varies from as low as 1 – 2 km at the northern and southern ends of our study area, to as high as 4 – 5 km in the central section west of Aceh, also characterised by the anomalous forearc morphology, and shallow compression within the downgoing plate.

5 Gravitational signature of prism collapse

The gravitationally-driven collapse of the forearc prism should be evident in gravity data, and indeed marine free-air gravity anomalies in the region also suggest that this region of the forearc is anomalous (Figure 1f). Gravity profiles across the trench typically show a wide gravity low centred on the trench itself, associated with the flexure of the downgoing plate, followed by a gradual rise to a gravity high at the peak of prism, as seen in the profiles for central Sumatra shown in Figure 2i,j. West of Aceh, however, the negative gravity anomaly associated with incoming plate flexure decays rapidly, and the profile rises sharply in the region of the trench itself, reaching a relative high $\sim$ 40 km landward of the trench (Central Section, Figure 2). The gravity profile then returns to a strong negative anomaly further landwards, over the low-gradient section of the forearc prism. The near-trench positive anomaly and prism-top negative anomaly match the gravity field expected for a region undergoing collapse due to gravitationally driven instability, as mass is rapidly moved from the wedge top to wedge front at a rate faster than the underlying plate can re-adjust.

In keeping with the uncertain nature of the near-trench seismicity in the northern section of our study area (Figure 3a), the gravitational profiles for this area (Figure 2b-d) shows a pattern similar to that for the area west of Aceh, but with a substantially smaller near-trench high. The regional tectonics in this area are further complicated by the transition to active N-S seafloor spreading behind the accretionary prism in the Andaman Sea. As a result, whilst the seismicity and gravity profiles are not representative of a typical subduction zone, without more data we are hesitant to ascribe this to collapse of the forearc, as we suggest is occurring west of Aceh.

6 Comparison to other subduction systems

Large-scale variations in the incoming sediment thickness to subduction systems also occur elsewhere on the planet, but the observed pattern of intraplate seismicity along the Sumatra margin remains unique. We ascribe this apparent contradiction to the relatively small proportion of the global subduction system to have sufficient outer rise seismicity to allow the type of detailed analysis presented here. Sections of several other subduction zones around the world, most notably Cascadia and the Chilean margin near Concepción, show similar forearc morphology variations to that seen west of Aceh, and have also been suggested to be undergoing forearc collapse (McNeill et al., 1997; Goldfinger et al., 2000; Geersen et al., 2011). However, relatively little intraplate seismicity has been observed along these margins during the instrumental period, and as such the intraplate strain is hard to assess. Hence, we suggest that when such seismicity does occur, likely in the period following a major earthquake on the adjacent subduction interface, the seismicity within the downgoing plate may show a pattern similar to that that we have observed west of Aceh.

Offshore northern Oregon and Washington, margin-perpendicular forearc extension from the late Miocene to present has produced normal faults within the sedimentary prism (McNeill et al., 1997). This process is limited to a region where the incoming plate surface is dominated by the major Astoria and Nitinat submarine fans, with incoming sediment thicknesses of 3–4 km, tapering away to both the south and north of the collapsing section of the margin (Goldfinger et al., 2012), suggesting that, as we infer for Sumatra, short-timescale variations in incoming sediment thickness can lead to rapid periods of forearc readjustment and collapse. Increased sediment thickness also has the effect of smoothing or masking the structure of the downgoing plate along the plate interface. This has been speculated to be a contributing factor in sustaining large, smooth ruptures during megathrust earthquakes, even in cases where the stress is lowered (Ruff, 1989) – a hypothesis that would fit with the spatial correlation of our suggested region of margin collapse with the region of highest slip in the 2004 Aceh-Andaman earthquake.

7 Conclusions

The seismicity of the near-trench region of the Sunda Arc west of Sumatra shows a notable departure from the global trend, with shallow compressional earthquakes occurring within the downgoing oceanic plate, in a region typically expected to be in horizontal extension. This region coincides with an area in which the forearc prism shows a steep front and low-angle top, characteristic of a region undergoing morphological readjustment in response to a change in the boundary conditions governing the shape of the accretionary prism. This change in prism morphology, with the prism propagating outwards over the downgoing plate, leads to closely-spaced regions of bending and unbending in the downgoing plate. The phase of prism collapse likely results from a rapid change in incoming sediment thickness and viscosity.

Acknowledgements

Seismogram data were retrieved from the IRIS Data Management Centre, and principally utilised networks II (doi:10.7914/SN/II), IU (doi:10.7914/SN/IU), GE (doi:10.14470/tr560404) and the network of the International Monitoring System. Data from regional seismic networks was also used where and when appropriate. A number of figures were made using the GMT software package. TJC was supported by a Research Fellowship from the Royal Commission for the Exhibition of 1851. This work forms part of the NERC- and ESRC-funded project 'Earthquakes without Frontiers', and AC was partly supported by the NERC grant 'Looking Inside the Continents from Space'. We thank Jon Bull for useful discussions, and we thank the editor and two anonymous reviewers for their thorough comments on the manuscript.

References

K. Aderhold and R. E. Abercrombie. Seismotectonics of a diffuse plate boundary: Observations off the Sumatra-Andaman trench. *Journal of Geophysical Research*, 121:3462–3478, 2016. doi: 10.1002/2015JB012721.

C. J. Ammon, C. Ji, H.-K. Thio, D. Robinson, S. Ni, V. Hjorleifsdottir, H. Kanamori, T. Lay, S. Das, D. Helmberger, G. Ichinose, J. Polet, and D. Wald. Rupture process of the 2004 Sumtra-Andaman Earthquake. *Science*, 308:1133–1139, 2005. doi: 10.1126/science.1112260.

H. Carton, S.C. Singh, N.D. Hananto, J. Martin, Y.S. Djajadihardja, Udrekh, D. Franke, and C. Gaedicke. Deep seismic reflection images of the Wharton Basin oceanic crust and uppermost mantle offshore Northern Sumatra: Relation with active and past deformation. *Journal of Geophysical Research*, 2014:32–51, 2014. doi: 10.1002/2013JB010291.

W. M. Chapple and D. W. Forsyth. Earthquakes and Bending of Plates and Trenches. *Journal of Geophysical Research*, 84:6729–6749, 1979.

A. P. S. Chauhan, S. C. Singh, N. D. Hananto, H. Carton, F. Klingelhoefer, J-X. Dessa, H. Permana, N. J. White, D. Graindorge, and Sumatra OBS Scientific Team. Seismic imaging of forearc backthrusts at northern Sumatra subduction zone. *Geophysical Journal International*, 179:1772–1780, 2009. doi: 10.1111/j.1365-246X.2009.04378.

M. Chlieh, J-P. Avouac, V. Hjorleifsdottir, T-R. A. Song, C. Ji, K. Sieh, A. Sladen, H. Hebert, L. Prawirodirdjo, Y. Bock, and J. Galetzka. Coseismic Slip and Afterslip of the Great M_W 9.15 Sumatra-Andaman Earthquake of 2004. *Bulletin of the Seismological Society of America*, 97:S152–S173, 2007. doi: 10.1785/0120050631.

D.H. Christensen and L.J. Ruff. Seismic coupling and outer rise earthquakes. *J. Geophys. Res.*, 93:13421–13444, 1988.

J.A.D. Connolly and Y.Y. Podladchikov. Temperature-dependent viscoelastic compaction and compartmentalization in sedimentary basins. *Tectonophysics*, 324:137–168, 2000.

B.J. Cook, T.J. Henstock, L.C. McNeill, and J. M. Bull. Controls on spatial and temporal evolution of prism faulting and relationships to plate boundary slip offshore north-central Sumatra. *Journal of Geophysical Research*, 119:5594–5612, 2014. doi: 10.1002/2013JB010834.

A. Copley and D. M^{c}Kenzie. Models of crustal flow in the India-Asia collision zone. *Geophysical Journal International*, 169:683–698, 2007. doi: 10.1111/j.1365-246X.2007.03343.x.

T. J. Craig, A. Copley, and J. Jackson. A reassessment of outer-rise seismicity and its implications for the mechanics of oceanic lithosphere. *Geophysical Journal International*, 197:63–89, 2014a. doi: 10.1093/gji/ggu013.

T. J. Craig, A. Copley, and T. A. Middleton. Constraining fault friction in oceanic lithosphere using the dip angles of newly-formed faults at outer rises. *Earth and Planetary Science Letters*, 392:94–99, 2014b. doi: 10.1016/j.epsl2014.02.024.

M. Delescluse and N. Chamot-Rooke. Instantaneous deformation and kinematics of the India-Australia Plate. *Geophysical Journal International*, 168:818–842, 2007. doi: 10.1111/j.1365-246X.2006.03181.x.

M. Delescluse, N. Chamot-Rooke, R. Cattin, L. Fleitout, O. Trubienko, and C. Vigny. April 2012 intra-oceanic seismcity off Sumatra boosted by the Banda-Aceh megathrust. *Nature*, 490:240–245, 2012. doi: 10.1038/nature11520.

C. DeMets, R. G. Gordon, and D. F. Angus. Geologically current plate motions. *Geophysical Journal International*, 181:1–80, 2010.

J.-X. Dessa, F. Klingelhoefer, D. Graindorge, C. André, H. Permana, M.-A. Gutscher, A. Chauhan, S. C. Singh, and the SUMATRA-OBS Scientific

Team. Megathrust earthquakes can nucleate in the forearc mantle: Evidence from the 2004 Sumatra event. *Geology*, 37:659–662, 2009. doi: 10.1130/G25653A.1.

J. W. Dewey, G. Choy, B. Presgrave, S. Sipkin, A. C. Tarr, H. Benz, P. Earle, and D. Wald. Seismicity associated with the Sumatra-Andaman Islands Earthquake of 26 December 2004. *Bulletin of Seismological Society of America*, 97:S25–S42, 2007. doi: 10.1785/0120050626.

E. R. Engdahl and C. H. Scholz. A double seismic zone beneath the central Aleutians: an unbending of the lithosphere. *Geophysical Research Letters*, 4:473–477, 1977.

E.R. Engdahl and S. Billington. Focal depth determination of Central Aleutian earthquakes. *Bulletin of the Seismological Society of America*, 76: 77–93, 1986.

P. England and D. McKenzie. A thin viscous sheet model for continental deformation. *Geophysical Journal International*, 70:295–321, 1982.

S. S. N. Gamage, N. Umino, A. Hasegawa, and S. H. Kirby. Offshore double-planed shallow seismic zone in the NE Japan forearc region revealed by sP depth phases recorded by regional networks. *Geophysical Journal International*, 178:195–214, 2009. doi: 10.1111/j.1365-246X.2009.04048.x.

J. Geersen, J.H. Behrmann, D. Völkerand S. Krastel, C. R. Ranero, J. Diaz-Naveas, and W. Weinrebe. Active tectonics of the South Chilean marine fore arc (35◦S–40◦S). *Tectonics*, 30, 2011. doi: 10.1029/2010TC002777.

C. Goldfinger, L. D. Kulm, L. C. McNeill, and P. Watts. Super-scale Failure of the Southern Oregon Cascadia Margin. *Pure and Applied Geophysics*, 157:1189–1226, 2000.

C. Goldfinger, C.H. Nelson, A.E. Morey, J.R. Johnson, J. Patton, E. Karabanov, J. Gutierrez-Pastor, A.T. Eriksson, E. Gracia, G. Dunhill, R. J. Enkin, A. Dallimore, and T. Vallier. Turbidite event history - Methods and implications for Holocene paleoseismicity of the Cascadia subduction zone. Professional Paper 1661-F, U.S.G Geological Survey, 2012.

D. Graindorge, F. Klingelhoefer, J-C. Sibuet, L. McNeill, T. J. Henstock, s. Dean, M-A. gutscher, J. X. Dessa, H. Permana, S. C. Singh, H. Leua, N. White, H. Carton, J. A. Malod, C. Rangin, K. G. Aryawan, A. K. Chaubey, A. Chauhan, D. R. Galih, C. J. Greenroyd, A. Laesanpura, J. Prihantono, G. Royle, and U. Shankar. Impact of lower plate structure on upper plate deformation at the NW Sumatran convergence margin from seafloor morphology. *Earth and Planetary Science Letters*, 275:201–210, 2008. doi: 10.1016/j.epsl.2008.04.053.

T.J. Henstock, L.C. McNeill, and D.R. Tappin. Seafloor morphology of the Sumatran subduction zone: Surface rupture during megathrust earthquakes? *Geology*, 34:485–488, 2008. doi: 10.1130/22426.1.

H. Kao and W-P. Chen. Seismicity in the outer rise-forearc region and configuration of the subducting lithosphere with special reference to the Japan Trench. *Journal of Geophysical Research*, 101:27811–27831, 1996.

A. O. Konca, V. Hjorleifsdottir, T-R. A. Song, J-P. Avouac, D. V. Helmberger, C. Ji, K. Sieh, R. Briggs, and A. Meltzner. Rupture Kinematics of the 2005 M_W 8.6 Nias-Simeulue Earthquake from the Joint Inversion of Seismic and Geodetic Data. *Bulletin of the Seismological Society of America*, pages S307–S322, 2007. doi: 10.1785/0120050632.

H. Kopp, W. Weinrebe, S. Ladage, U. Barckhausen, D. Klaeschen, E.R. Flueh, C. Gaedicke, Y. Djajadihardja, I. Grevemeyer, A. Krabbenhoeft, C. Papenberg, and M. Zillmer. Lower slope morphology of the Sumatra Trench. *Basin Research*, 20:519–529, 2008. doi: 10.1111/j.1365-2117.2008.00381.x.

D. Lange, F. Tilmann, A. Rietbrock, R. Collings, D. H. Natawidjaja, B. W. Suwargadi, P. Barton, T. Henstock, and T. Ryberg. The Fine Structure of the Subducted Investigator Fracture Zone in Western Sumatra as seen by Local Seismicity. *Geophysical Journal International*, 298:47–56, 2010. doi: 10.1016/j.epsl.2010.07.020.

T. Lay, L. Astiz, H. Kanamori, and D. H. Christensen. Temporal variation of large intraplate earthquakes in coupled subduction zones. *Physics of the Earth and Planetary Interiors*, 54:258–312, 1989.

T. Lay, H. Kanamori, C. J. Ammon, A. R. Hutko, K. Furlong, and L. Rivera. The 2006-2007 Kuril Islands great earthquake sequence. *Journal of Geophysical Research*, 114, 2009. doi: 10.1029/2008JB006280.

J.-Y. Lin, X. Le Pichon, C. Rangin, J.-C. Sibuet, and T. Maury. Spatial afterhshock distribution of the 26 December 2004 great Sumatra-Andaman earthquake in the northern Sumatra area. *Geochemistry, Geophysics, Geosystems*, 10, 2009. doi: 10.1029/2009GC002454.

D. McKenzie and J. Jackson. Tsunami earthquake generation by the release of gravitational potential energy. *Earth and Planetary Science Letters*, 345-348:1–8, 2012. doi: 10.1016/j.epsl.2012.06.036.

L. McNeill and T. J. Henstock. Forearc structure and morphology along the Sumatra-Andaman subduction zone. *Tectonics*, 33:112–134, 2014. doi: 10.1002/2012TC003264.

L.C. McNeill, K. A. Piper, C. Goldfinger, and L. D. Kulm. Listric normal faulting on the Cascadia continental margin. *Journal of Geophysical Research*, 102:12123–12138, 1997.

R. Moeremans, S. Singh, M. Mukti, J. McArdle, and K. Johansen. Seismic images of structural variations along the deformation front of the Andaman-Sumatra subduction zone: Implications for rupture propagation and tsunamigenesis. *Earth and Planetary Science Letters*, 386:75–85, 2014. doi: 10.1016/j.epsl.2013.1.1003.

P. Molnar and H. Lyon-Caen. Fault plane solutions of earthquakes and active tectonics of the Tibetan Plateau and its margins. *Geophys. J. Int.*, 99:123–153, 1989.

K. Reynolds, A. Copley, and E. Hussain. Evolution and dynamics of a fold-thrust belt: the Sulaiman Range of Pakistan. *Geophysical Journal International*, 201:683–710, 2015. doi: 10.1093/gji/ggv005.

J. Rhie, D. Dreger, R. Bürgmann, and B. Romanowicz. Slip of the 2004 Sumatra-Andaman Earthquake from Joint Inversion of Long-Period Global Seismic Waveforms and GPS Static Offsets. *Bulletin of the Seismological Society of America*, 97:S115–S127, 2007. doi: 10.1785/0120050620.

L.J. Ruff. Do Trench Sediments Affect Great Earthquake Occurrence in Subduction Zones? *Pure and Applied Geophysics*, 129:263–283, 1989.

E.H. Rutter. Pressure solution in nature, theory and experiment. *Journal of the Geological Society of London*, 140:725–740, 1983.

D. Sandwell and W. H. F. Smith. Global marine gravity from retracked Geosat and ERS-1 altimetry: Ridge segmentation versus spreading rate. *Journal of Geophysical Research*, 114, 2009. doi: 10.1029/2008JB006008.

S. C. Singh, H. Carton, P. Tapponnier, N. D. Hananto, A. P. S. Chauhan, D. Hartoyo, M. Mayly, S. Moeljopranoto, T. Bunting, P. Christie, H. Lubis, and J. Martin. Seismic evidence for broken oceanic crust in the 2004 Sumatra earthquake epicentral region. *Nature Geoscience*, 1, 2008. doi: 10.1038/ngeo336.

S. C. Singh, A. P. S. Chauhan, A. J. Calvert, N. D. Hananto, D. Ghosal, A. Rai, and H. Carton. Seismic evidence fo bending and unbending of subducting oceanic crust and the presence of mantle megathrust in the 2004 Great Sumatra earthquake rupture zone. *Earth and Planetary Science Letters*, 321-322:166–176, 2012. doi: 10.1016/j.epsl.2012.01.012.

T. Taymaz, J. Jackson, and D. McKenzie. Active tectonics of the north and central Aegean Sea. *Geophysical Journal International*, 106:433–490, 1991.

F. J. Tilmann, T. J. Craig, I. Grevemeyer, B. Suwargadi, H. Kopp, and E. Flueh. The updip seismic/aseismic transition of the Sumatra megathrust illuminated by aftershocks of the 2004 Aceh-Andaman and 2005 Nias events. *Geophysical Journal International*, 181:1261–1274, 2010. doi: 10.1111/j.1365-246X.2010.04597.x.

F. Waldhauser, D. P. Schaff, T. Diehl, and E. R. Engdahl. Splay Faults imaged by fluid-driven aftershocks of the 2004 M_W 9.2 Sumatra-Andaman earthquake. *Geology*, 40:243–246, 2012. doi: 10.1130/G32420.1.

D. A. Wiens, C. DeMets, R. G. Gordon, S. Stein, D. Argus, J.F. Engeln, P. Lundgren, D. Quible, C. Stein, S. Weinstein, and D.F. Woods. A Diffuse plate boundary model for Indian Ocean tectonics. *Geophysical Research Letters*, 12:429–432, 1985.

W-C. Yu, T-R. A. Song, and P. G. Silver. Repeating aftershocks of the great 2004 Sumatra and 2005 Nias earthquakes. *Journal of Asian Earth Sciences*, 67-68:153–170, 2013. doi: 10.1016/j.jseaes.2013.02.018.

H. Yue, T. Lay, and K. D. Koper. *En échelon* and orthogonal fault ruptures of the 11 April 2012 great intraplate earthquakes. *Nature*, 490:245–251, 2012. doi: 10.1038/nature11492.

P. Zwick, R. McCaffrey, and G. Abers. MT5 program. *IASPEI Software Library*, 4, 1994.

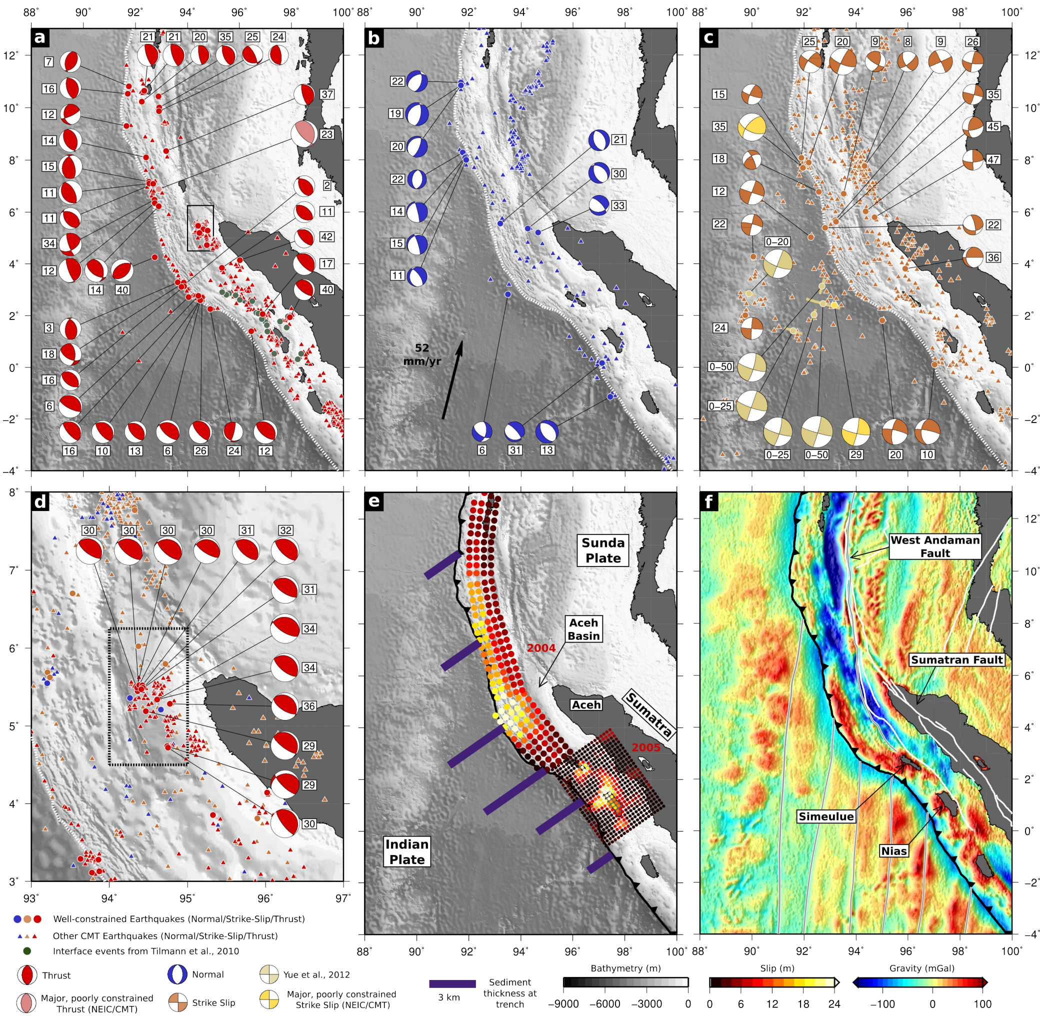

Figure 1: Seismic activity and plate structure west of Sumatra. Earthquakes with well-constrained source parameters from this study are plotted as circles, with associated focal mechanisms. The depth beneath the seabed of each earthquake is given by the number next to the mechanism. Events from the gCMT catalogue are shown as triangles, for those earthquakes occurring within 100 km seawards, and 300 km landwards, of the trench. (a) Thrust-faulting earthquakes. Green points are the low-angle interface events of Tilmann et al. (2010). Earthquakes within the dashed box are shown in (d). (b) Normal-faulting earthquakes. The black arrow is the convergence vector between the Indian plate and the Sunda plate (DeMets et al., 2010). (c) Strike-slip faulting earthquakes. Beige mechanisms are sub-events of the 2012 Indian Ocean earthquake (Yue et al., 2012), with bars indicative of along strike extent of rupture, and depth ranges indicative of the depth range of major slip in finite-fault models. (d) Thrust-faulting earthquakes in the Aceh Basin. (e) Slip models for the 2004 Aceh-Andaman (Rhie et al., 2007) and 2005 Nias (Konca et al., 2007) earthquakes. The slip magnitudes for the Nias event have been multiplied by a factor of 3 relative to the Aceh-Andaman event, to make the two events visible on the same colour scale. Sediment thicknesses seaward of the trench are shown by the thick purple bars (McNeill and Henstock, 2014, and references therein). (f) Free-air gravity anomalies (Sandwell and Smith, 2009). Grey and white lines mark fracture zones in the Indian plate, and major strike slip fault systems in the overriding plate.

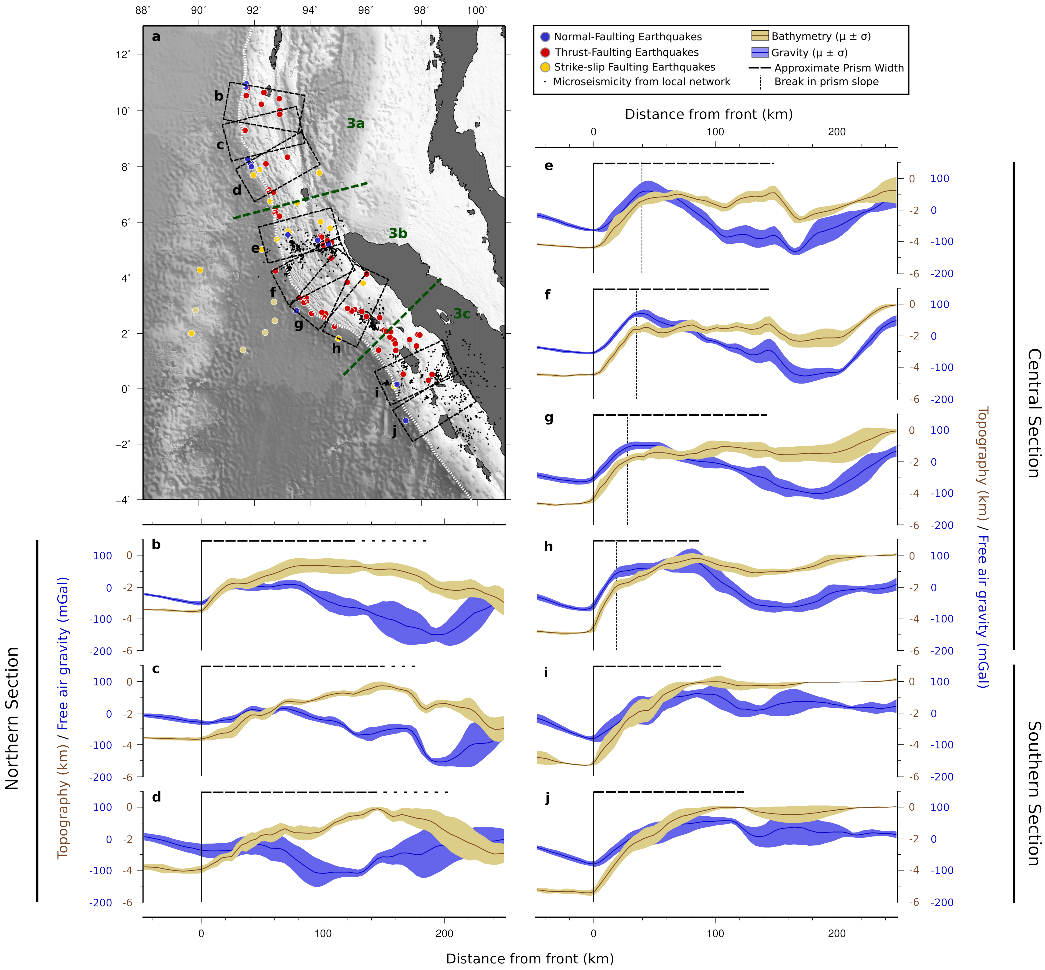

Figure 2: (a) Map of earthquakes with well-constrained depths, coloured by mechanism. Black points are microseismic activity from local seismic deployments (Lin et al., 2009; Tilmann et al., 2010; Lange et al., 2010). Black dashed boxes are the areas used for swaths of bathymetric and gravity data shown in (b) – (j). Green dashed lines separate the regions used for the cross-sections shown in Figure 3. (b) – (j) show mean (darker line) and $\pm 1\sigma$ values (shaded bands) for the trench-perpendicular swaths shown on (a). Beige/brown are for bathymetric/topographic data, blues are for free-air gravity data. Vertical solid lines indicate the location of the trench. Vertical dashed lines on (e) – (j) indicate the principal break in slope. Horizontal dashed lines indicate the approximate prism width in each case (the western prism boundary on (b) – (d) is uncertain).

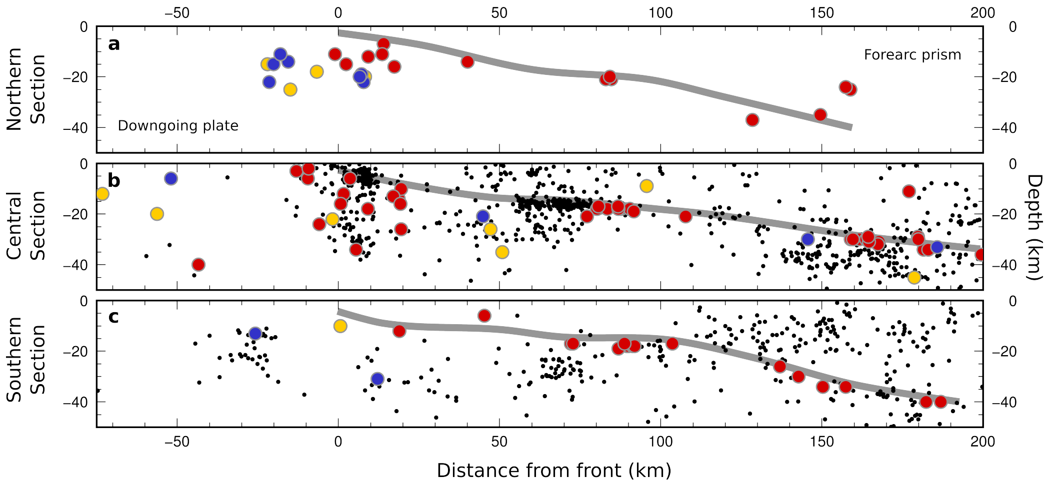

Figure 3: Cross-sections through earthquakes north of the green line on Figure 2a intersecting the trench at 6.5°N (e), between the two green lines (f) and south of the green line intersecting the trench at 1.5°N. All earthquakes are shown at their minimum trench-perpendicular distance. Red points are thrust-faulting earthquakes, blue are normal-faulting earthquakes, and yellow are strike-slip faulting earthquakes (as on Figure 2a). Small black points are earthquake hypocentres from local seismic network deployments, as shown on Figure 2a. Depth is indicative of their depth below sea level.

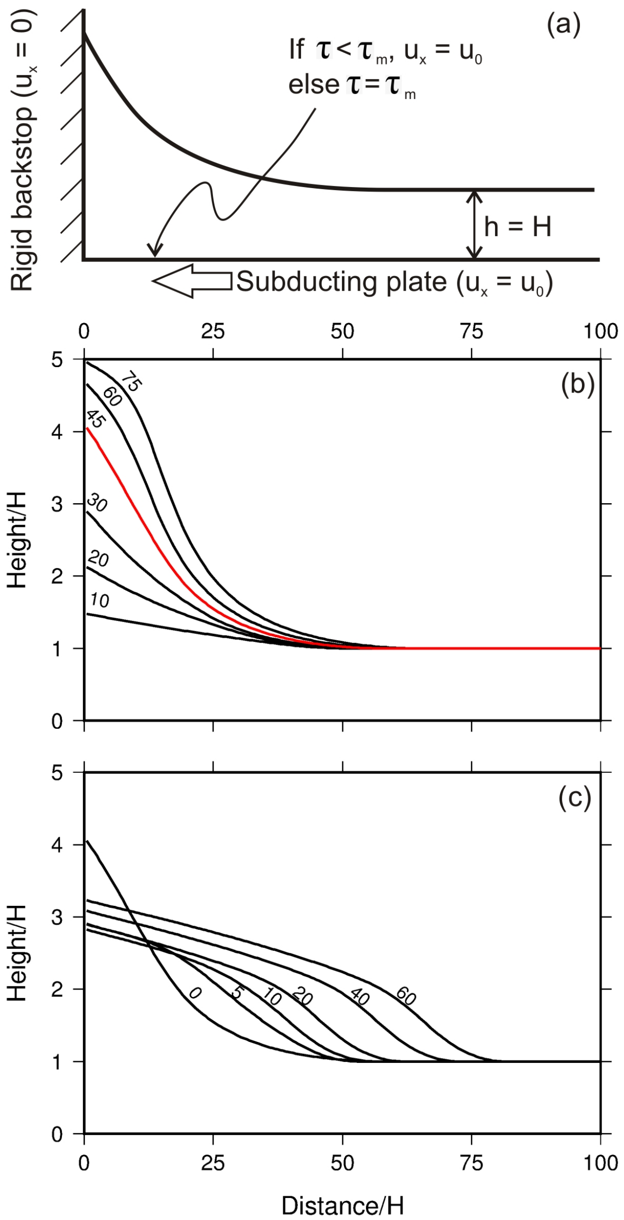

Figure 4: Modelling forearc evolution. (a) model setup. (b) model results for α=15 and τ_m = 0.05. These values are equivalent to a wedge viscosity of 2×10^{20}Pa s and a megathrust shear stress of 16 MPa, for a convergence rate of 52 mm/yr, sediment thickness of 1 km, and density of 2500 kg/m^3. This viscosity is similar to that which Copley and M^{c}Kenzie (2007) found for the onshore Indo-Burman sedimentary wedge, and the shear stress is similar to the stress-drops observed in megathrust earthquakes. The curves show the topography labelled with non-dimensionalised time. For the parameters chosen, a non-dimensional time of 45 is equivalent to $\sim$900 kyr. (c) Model results when the red curve in (b) is taken as a starting configuration, and the value of α is reduced by a factor of 10.

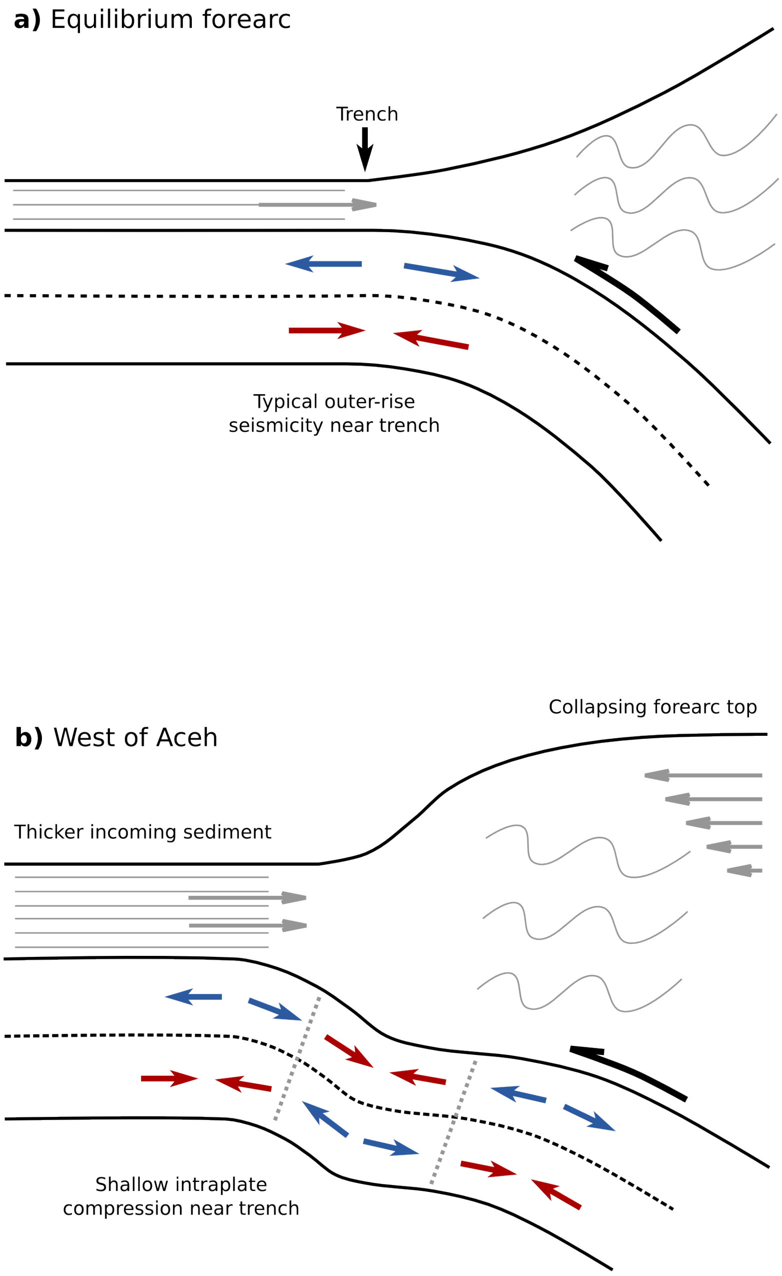

Figure 5: Schematic diagram linking forearc morphology and bending strains within the downgoing plate. (a) The globally-typical scenario for forearcs in equilibrium. (b) The scenario we propose for the Sunda arc west of Aceh during forearc readjustment.